Supercritical Fluid-Liquid-Solid Growth of Alloyed $Si_{1-x}Ge_x$ Nanowires

Ge Gu

A thesis

submitted in partial fulfillment of the

requirements for the degree of

Master of Science in Chemical Engineering

University of Washington

2020

Reading Committee:

Vincent C. Holmberg, Chair

Qiuming Yu

Program Authorized to Offer Degree:

Chemical Engineering

University of Washington

Abstract

Supercritical Fluid-Liquid-Solid Growth of Alloyed $Si_{1-x}Ge_x$ Nanowires

Ge Gu

Chair of the Supervisory Committee:
Assistant Professor Vincent C. Holmberg
Department of Chemical Engineering

Silicon (Si) and germanium (Ge) have emerged as next-generation anode materials for Li-ion batteries due to their high theoretical capacities (Si:3579mAh/g, Ge:1384mAh/g) and are promising replacements for lower-capacity, graphite-based anodes (372mAh/g). However, one significant challenge of their practical implementation is the large volume change associated with the insertion and extraction of lithium ions, which results in mechanical pulverization and capacity fade. Nanostructuring active material morphology has been demonstrated as a strategy to compensate for volume change and improve capacity and cycle life in lithium ion batteries.

Although Si has the highest theoretical capacity among elemental lithium ion battery negative electrodes and maintains distinct advantages as an electrode material, silicon's rate capability is

hindered by its lower ionic diffusivity and electronic conductivity in comparison to Ge. However, Ge is much more expensive, which could limit its widespread use in anodes for lithium ion batteries. In an effort to capitalize on the benefits of both materials, there has been recent interest in developing an anode that combines the excellent rate capability of Ge with the high capacity and lower cost of Si. Recent efforts have demonstrated the ability to synthesize alloyed $Si_{1-x}Ge_x$ nanowires (NWs) via a solution-based mechanism, using a thin film of tin to seed nanowire growth.

In order to improve the scalability of this process, here we report the supercritical fluid-based synthesis of Sn nanocrystal-seeded alloyed $Si_{1-x}Ge_x$ NWs. By balancing reaction parameters such as precursor reactivity, the semiconductor precursor to metal seed ratio, Si:Ge precursor ratio, and reaction temperature, we demonstrate the ability to synthesize alloyed $Si_{1-x}Ge_x$ NWs through a colloidal, supercritical fluid-based process for the first time.

TABLE OF CONTENTS

LIST OF FIGURES

ACKNOWLEDGEMENTS

I want to thank for everyone who helped me with my project and study during these two years in UW. First, I would like to express my very great appreciation to Professor Vincent Holmberg for his valuable and constructive suggestions during the planning and development of this research work. I would also like to thank Dr. Elena Pandres, for her advice and assistance in keeping my progress on schedule. Her patient guidance, enthusiastic encouragement and useful critiques of this research work are really valuable for this project. I am also appreciative of Yao-Yu Li and his hard work in supporting recent experiments. Thank you to all the members in the research group, including Soohyung Lee, Brittany Bishop, Guesang Kevin Lee, Yao-Yu Li, and Chih-Wei Hsu for your help and support.

I would also like to extend my thanks to my friends for their scientific and moral support. I want to thank Zonglun Li and Zizhao Xu for sharing their knowledge of Raman Scattering and nanomaterials. I also want to thank you for your support during the outbreak in the experiments. You were always willing to chat with me and share your incredible ideas in leisure time. Thank you for helping me feel comfortable and release in this tedious time.

Finally, I want to appreciate my parents for supporting my study in UW, without whom none of these would happen. Thank you for your unconditional love and support throughout my life.

Chapter 1. INTRODUCTION

1.1 NANOMATERIALS FOR LITHIUM ION BATTERIES

Lithium-ion Batteries (LIBs) have attracted considerable attention in recent years due to their potential impact in many diverse applications such as electric vehicles (EVs), laptops, and mobile phones. In particular, silicon (Si) and germanium (Ge) have emerged as promising alternative anode materials to replace graphite, which only has a theoretical capacity of 372mAh/g). Si and Ge have much higher theoretical capacities (Si:3579mAh/g, Ge:1384mAh/g),[1,2] but there are still many challenges for the practical implementation of these new anode materials.

One significant challenge of the alloying materials in LIBs is the large volume change associated with the insertion and extraction of lithium ions, which results in mechanical pulverization due to the strain and stress.[3–6] For example, Si undergoes large variations in volume during the lithiation and delithiation processes (>300%), which contributes to capacity fade in a number of ways.[7] The drastic volume changes cause strain, which results in electrode fracture and even delamination of the electrode from the current collector. In addition, during cycling, decomposition of the organic electrolyte occurs at the electrode-electrolyte interface to form the solid electrolyte interphase (SEI) layer, which plays a key role in battery function. The SEI layer should be thin robust; ideally, it is ionically conductive and electronically insulating. However, the large volume change associated with alloying electrode materials such as Si and Ge, makes it challenging to form a robust SEI layer. The initial SEI layer may crack as the Si or Ge expands and contracts repeatedly throughout cycling. When fresh Si surface is exposed, the electrolyte decomposes at the electrode surface to form a new SEI layer, resulting in further

deleterious side reactions that trap the mobile ion.[7] This process happens iteratively and can result in a thicker SEI layer throughout cycling, ultimately causing capacity fade.

A wide range of strategies have been developed to address these issues, including nanostructuring the electrode active material in order to reduce the strain that results in electrode fracture. Various morphologies, including thin films, nanoparticles, nanotubes, and coral-like structures, have been investigated for alloying electrode materials such as Si and Ge.[4,8–10] Notably, Chan, *et al.* proposed using Si nanowires (Si NWs) as anodes in LIBs.[11] The nanowire morphology has since been shown to accommodate the large volume changes associated with lithiation and delithiation.[3,12] In particular, Chan, *et al.* demonstrated that Si NW battery anodes could retain a discharge capacity at around 3200mAh/g after 10 cycles with minimal capacity fade. Si NWs can radially accommodate the strain associated with lithiation and maintain their morphology, compared to Si thin films or microparticles, which fracture during cycling.[13–15]

Even though Ge has a lower theoretical lithiation capacity than Si, it still has over three times the theoretical capacity than graphite. In addition, Ge has unique properties that make it a promising material for lithium-ion battery applications that require high power density. In particular, Ge has a high electrical conductivity (1000X) and high ion conductivity of Li (400X), which results in a much better rate capability compared to Si.[16–21] Ge nanowire-based electrodes have exhibited good capacity retention and high rate capability, which has been attributed to the electrochemically-activated formation of a porous network to facilitate ion and electron transport.[21]

1.2 STRATEGIES TO PRODUCE NANOWIRES

The vapor-liquid-solid mechanism remains one of the most common approaches to fabricate semiconductor nanowires.[22–26] It was initially demonstrated by Wagner and Ellis[27], who grew single-crystal Si wires by using gold as a seed to lower the energy barrier to crystallization.

In VLS growth of Si wires, a thin film of gold (Au) is typically evaporated onto a substrate, which is placed in a chemical vapor deposition chamber. As the chamber temperature increases and as the Si precursor is introduced in the vapor phase, the gold film dewets to form Au-Si alloy droplets. As the flow of the Si precursor continues into the chamber, the concentration of Si atoms increases in the alloy droplet. Eventually, the alloy droplets become supersaturated with Si, causing Si to precipitate and crystallize at the droplets surface, facilitating anisotropic growth of crystalline Si.[27]

A variety of vapor-based synthetic methods on the VLS mechanism have been developed for semiconductor nanowire growth, including chemical deposition techniques (chemical vapor deposition and molecular beam epitaxy)[28–33] and physical deposition techniques (laser ablation)[34–37]. VLS has many advantages, such as the ability to produce high-quality, well-aligned nanowire as well as the ability to have well-defined control of the nanowire composition.[38] In addition, studies about how vapor-based reaction conditions affect nanowire growth direction, phase, and composition have been especially important for understanding fundamental mechanisms of semiconductor nanowire growth processes.[39–41] However, VLS-based nanowire growth typically requires vacuum-based equipment, is performed in a batch reaction, and is typically limited to producing micrograms of material, all of which make it difficult to scale vapor-based nanowire growth processes in a cost-effective manner.

Another strategy, Solution-Liquid-Solid (SLS) nanowire growth, was developed in 1995.[42] It is similar to the VLS approach, but it introduces the semiconductor precursor in solution, rather than in the vapor phase. In VLS, the metal seed source is limited to the area of the substrate, which means that nanowire growth is limited to batch growth on the area of the substrate. In SLS nanowire growth, metal nanocrystal seeds are dispersed in solution, which enables nanowire growth throughout the entire volume of the solution-phase reaction, thereby improving scalability. SLS also has somewhat improved control over surface passivation and can produce nanowires with diameters below 10 nm.[43]

The metal seed selection for SLS-based nanowire growth is also important in terms of the melting point and semiconductor solubility. While SLS methods have been successful in synthesizing a wide range of nanowire compositions and phases with narrow diameter distributions, SLS-based nanowire growth still has some limitations.[44] The chemistries available to SLS-based nanowire growth are limited by solvent boiling points, which is typically around a maximum of 400°C, meaning that only low-melting-point metal nanoparticles can be used as catalysts. Ga, In, Sn and Bi have been widely used in SLS growth of semiconductor materials under certain conditions.[45–50] Although Au seeds are widely used in VLS and Au nanoparticles are easy to synthesize on the benchtop, the high-melting point of gold and the high eutectic temperature of Au with semiconductor materials, have limited its use in SLS-based nanowire growth. Besides, Au is not electrochemically active; in fact, Au dopants in semiconductor nanowires actually create deep traps that are detrimental to the electrical properties of the nanowires, which has a negative impact on battery performance.[51] Therefore, when choosing a metallic seed, the incorporation of dopant atoms from the metal seed into the semiconductor nanowires should be considered as well. Another noteworthy point is the semiconductor atom

solubility in the metal seed. During the nanowire growth process, the low solubilities of the semiconductor component in the alloyed droplet may facilitate faster supersaturation.

Supercritical Fluid-Liquid-Solid (SFLS) is another solution-based nanowire growth method, in which the semiconductor precursor is introduced in the supercritical fluid phase. In SFLS, the maximum temperature for reactions is not limited by the boiling point of the solvent, thereby expanding the range of chemistries possible in this high pressure, high temperature system. In addition, supercritical fluid-based nanowire growth typically operates in continuous flow and produces much higher yields of nanowires, thereby improving the potential for scalability. The supercritical reactor consists of a 10 mL high-pressure cylindrical titanium vessel and two valves at both inlet and outlet. A reactor filled with nitrogen is placed inside a heating block. A thermocouple placed between the reactor and heating block, which is connected to a temperature controller, allows users to control the heating rate of the system. The inlet of the reactor was connected to a 6-way valve and the outlet is connected to a micrometering valve, which can manually control the pressure of the system. A high-pressure liquid chromatography (HPLC) pump is used to pressurize the system by pushing water into a tall cylinder, which is filled with anhydrous toluene and connected to inline of the 6-way valve. There is a pressure sensor between the tall cylinder and the 6-way valve monitoring the pressure and a rupture discs to protect the whole system from over-pressuring. The Korgel group first demonstrated the synthesis of Si nanowires via supercritical fluid-based growth in 2000.[48] Si nanowires were grown from 2.5 nm diameter Au nanocrystals in supercritical hexane at 500°C with diphenylsilane as the Si precursor. The resulting nanowires had lengths up to several micrometers and diameters with a narrow size distribution.[48] Since then, a variety of nanowire compositions have been grown via supercritical fluid-based methods, such as Ge, GaAs, GaP, InP, InAs, and CdSe.[50,52–54] Si and Ge nanowires synthesized via supercritical fluid methods have

also been successfully employed as the active material in lithium ion battery anodes and have exhibited a good performance.[55–57] In fact, supercritical fluid-grown Si nanowires have been used to create nonwoven fabrics, which can then be used as binder-free anodes for lithium ion batteries.[58]

1.3 ALLOYED SILICON-GERMANIUM NANOMATERIALS

Although Si has the highest theoretical capacity for lithium ion batteries and maintains distinct advantages as an electrode material, it also has a lower ionic diffusivity and electronic conductivity which results in worse rate capability when compared to Ge. However, Ge is much more expensive, which could limit its widespread use in anodes for lithium ion batteries. In an effort to capitalize on the benefits of both materials, there has been recent interest in developing an anode that combines the excellent rate capability of Ge with the high capacity and lower cost of Si.

One strategy is to incorporate these two materials into one electrode material. Several groups have synthesized various alloyed silicon-germanium material systems and tested the capacity and rate capability.[10,59–64] For example, $Si_{1-x}Ge_x$ thin films synthesized by glancing angle deposition exhibited tunable gravimetric capacity and rate capability by adjusting the Si: Ge composition ratio.[10] Stokes, *et al.* developed an approach to fabricate a Si-Ge branched NW heterostructure.[64] As an electrode, the Si-Ge branched NW heterostructure demonstrated high capacity and good capacity retention. In general, as the Ge concentration increases in alloyed Si: Ge materials, the electrodes show much better capacity retention at faster cycling rates.

Recently, $Si_{1-x}Ge_x$ alloyed NWs were grown via the SLS mechanism, using tin as the metal seed. Moreover, the Si: Ge atomic ratio was tunable by varying the ratio of Si and Ge precursors in solution.[63] The resulting alloyed $Si_{1-x}Ge_x$ NWs exhibited a tunable rate capability

and gravimetric capacity as a function of the Si: Ge ratio. Although this particular process introduced the semiconductor precursors in the solution phase, it used a thin film of evaporated tin onto a substrate as the source of tin in order to grow nanowires directly from the substrate.[63] Seed selection is a critical aspect of $Si_{1-x}Ge_x$ nanowire synthesis. By strategically selecting a metal seed that is both electrochemically active and also forms a ternary alloy with Si and Ge, the metal seed not only facilitates alloyed nanowire growth, but it also contributes to the gravimetric capacity. Several metallic seeds have been introduced in the past for synthesizing semiconductor nanowires such as Au, Ni, Al, Cu, Bi, In, Fe.[47,49,65,66] By using tin as the seed, which has a theoretical capacity of 992 mAh/g,[56,63] the seed actually contributes to the performance of the electrode, rather than being detrimental to the battery performance. While growing $Si_{1-x}Ge_x$ NW directly from the current collector permits fast electron transport, nanowire growth from a substrate also limits the total mass loading of active and reduces the potential scalability of the synthesis.

Translating this substrate-based SLS synthesis of $Si_{1-x}Ge_x$ NWs to supercritical fluid-based method, could improve its scalability. Here, we report recent developments of the supercritical fluid-based synthesis of Sn-seeded $Si_{1-x}Ge_x$ alloyed NWs. To our knowledge, this is the first demonstration of supercritical fluid-based techniques to produce alloyed Group IV semiconductor nanowires.

Chapter 2. EXPERIMENT DETAILS

2.1 MATERIALS AND REAGENTS

Lithium bis(trimethylsilyl)amide ($LiN(SiMe_3)_2$, 97%, Aldrich), oleic acid (degassed, 90%, Aldrich), tin (II) chloride ($SnCl_2$, anhydrous, ≥99.99%, trace metals basis, Aldrich), tetrachloroethylene (TCE, ≥99%, Aldrich), lithium triethylborohydride (also known as superhydride, Li(Et3BH), 1.0 M solution in tetrahydrofuran, Aldrich), oleylamine (90%, Aldrich), chloroform (HPLC grade, 99.9%, Fisher), ethanol (100%, Fisher), toluene (≥99.5%, Fisher), monophenylsilane (PS, >95%, Gelest), triphenylgermane (TPG, >97%, Gelest), anhydrous toluene (99.8%, Gelest) were used as received.

2.2 NANOMATERIAL SYNTHESIS

2.2.1 *Sn Nanocrystal synthesis*

A nitrogen glove box was used to store and handle all air- and moisture-sensitive chemicals. All syntheses were carried out under nitrogen atmosphere using standard Schlenk line techniques.

The synthesis of Sn NCs was performed using the method of Kravchyk *et al.*[67] In a typical synthesis of 9-nm Sn NCs, 16 mL oleylamine was loaded in a three-neck round bottom flask. The flask was purged of air for five minutes on the Schlenk line while stirring at 1000 RPM. The mixture underwent a cycling process between vacuum and nitrogen three times. The solution was heated up to 140℃ and dried under vacuum for 1.5 hours under constant stirring at 1000 RPM. Afterward, oleylamine was cooled down to 50℃, and 0.5 mmol $SnCl_2$ was added to the flask followed by another drying under vacuum for 0.5 h at 140℃. Meanwhile, 3.6 mmol

$LiN(SiMe_3)_2$ was dissolved in 2 mL toluene in the glove box and loaded into a syringe. Additionally, 0.6 mL of the superhydride solution was loaded into a syringe. Then the $SnCl_2$/oleylamine mixture was heated up to 180°C under nitrogen, and $LiN(SiMe_3)_2$/toluene solution was injected into the flask. In 10 s, 0.6 mL of the superhydride solution was injected into the flask. The color of the solution should immediately turn dark brown. The reaction proceeded for one hour, and the flask was removed from the heating mantle. When the temperature reached 120-150°C, 10 mL of anhydrous toluene was added to the reaction solution, and then the flask was rapidly cooled down to room temperature by submersion in an ice-water bath. After cooling, the flask was transferred into a glove box, which is where all nanocrystal washing was performed. The nanocrystals were precipitated by adding 40 mL of ethanol, followed by centrifugation at 8000 RPM for 4 minutes. The supernatant was discarded, and the nanocrystals were redispersed in tetrachloroethylene (5 mL) and oleic acid (1 mL) in order to replace the weakly bound oleylamine. 10 mL of ethanol were added, and the Sn NCs were precipitated by centrifugation again. The supernatant was discarded and the, Sn NCs were redispersed in a nonpolar solvent such as toluene and stored in a glovebox.

2.2.2 *$Si_{(1-x)}Ge_x$ nanowires synthesis*

In a typical $Si_{1-x}Ge_x$ NW synthesis, a 10 mL solution of anhydrous toluene containing 0.27 mg/mL Sn nanocrystals, 90 mM phenylsilane and, 5.4 mM triphenylgermane were loaded into a syringe in a nitrogen-filled glove box. Meanwhile, a nitrogen-filled titanium tubular reactor was transferred into a nitrogen atmosphere, sealed, placed in a heating box and then heated to 490°C. Anhydrous toluene was continuously flowed into the reactor at a rate at 0.5 mL/min until a pressure of 900 psig was reached. After that, the inlet valve of the reactor was

closed, resulting in a pressurized reactor. The solution in the syringe was loaded into a 10 mL injection coil. Then the 6-way valve was switched to flow anhydrous toluene into the coil containing the precursors, pressurizing the injection loop 900 psig. The reactor inlet valve was opened and the precursors in the injection loop were introduced into the reactor at a flow rate of 0.5 mL/min for 20 min. During the reaction process, the outlet valve was left open and the micrometering valve was controlled manually to maintain a steady-state pressure at 900 psig in the reactor.

After 20 minutes, both the outlet and inlet valves were closed, and the reactor was removed from the heating block and cooled to room temperature. Then the reactor was opened at ambient conditions and the nanowires were collected. The nanowires were precipitated by centrifugation at 8,000 rpm for 5 min. The supernatant was discarded. The nanowires were redispersed in 10 mL of chloroform. 10 mL of toluene and 5 mL of ethanol were added prior to centrifugation to crash the nanowires down again. After repeating the washing procedure three times, the nanowires were stored in 20 mL toluene for later use.

2.3 CHARACTERIZATION METHODS

2.3.1 *Scanning Electron Microscopy (SEM)*

SEM samples were prepared by dropping 15 μL of dilute nanowires dispersed in toluene onto aluminum foil. Samples were imaged using a Sirion XL30 scanning electron microscopy. Energy-dispersive X-ray spectroscopy (EDS) was carried out using a scanning electron microscope (XL30) equipped with an X-ray energy-dispersive spectroscopy detector in order to analyze the composition of $Si_{1-x}Ge_x$ nanowires dropped onto an aluminum foil.

2.3.2 *Transmission Electron Microscopy (TEM)*

Sn nanocrystals were prepared for TEM by dropping 10 μL of the Sn nanocrystal dispersion onto an ultrathin carbon TEM grid placed on top of a piece of filter paper. TEM images were acquired with a FEI Tecnai G2 F20 Supertwin TEM, operating at 200 kV. Fast Fourier Transforms (FFTs) of high-resolution TEM images were generated by Digital Micrograph Software.

2.3.3 *X-Ray Diffraction (XRD)*

XRD sample preparation of Sn nanocrystals was performed by dropping 5 μL increments of the Sn nanocrystal dispersion onto a silicon substrate until 75 μL were dried in one spot. XRD samples of $Si_{1-x}Ge_x$ nanowires were prepared by depositing 10 μL of the $Si_{1-x}Ge_x$ nanowire dispersion onto aluminum foil iteratively and allowing the droplet to dry five times. XRD were collected with a Bruker D8 Discover equipped with an IμS 2-D XRD detector system and were analyzed with EVA software.

2.3.4 *Raman Spectroscopy*

$Si_{1-x}Ge_x$ nanowires were prepared for Raman spectroscopy by dropping 10 μL of the nanowire dispersion onto a glass slide five times in the same spot, allowing the droplet to dry before depositing a new droplet. Raman spectra were collected using a Thermo Scientific DXR2 Raman microscope, with an excitation wavelength of 523nm at a power of 1mW for one minute.

Chapter 3. RESULTS AND DISCUSSION

3.1 SUPERCRITICAL FLUID-BASED SYNTHESIS OF $Si_{1-x}Ge_x$ NANOWIRES

To synthesize $Si_{1-x}Ge_x$ nanowires via supercritical fluid-based methods, a mixture consisting of tin nanocrystals, monophenylsilane, and triphenylgermane was injected at a consistent flow rate into a reactor at high-pressure (900 psig) and high-temperatures (460-500°C). Figure 1a and Figure 1b show TEM of the colloidal tin nanocrystals used as seeds to synthesize alloyed $Si_{1-x}Ge_x$ nanowires; their size distribution had a standard deviation less than 30% about mean diameter at about 20 nm. Figure 1c is XRD data of the nanocrystals, confirming that they are composed of tin.

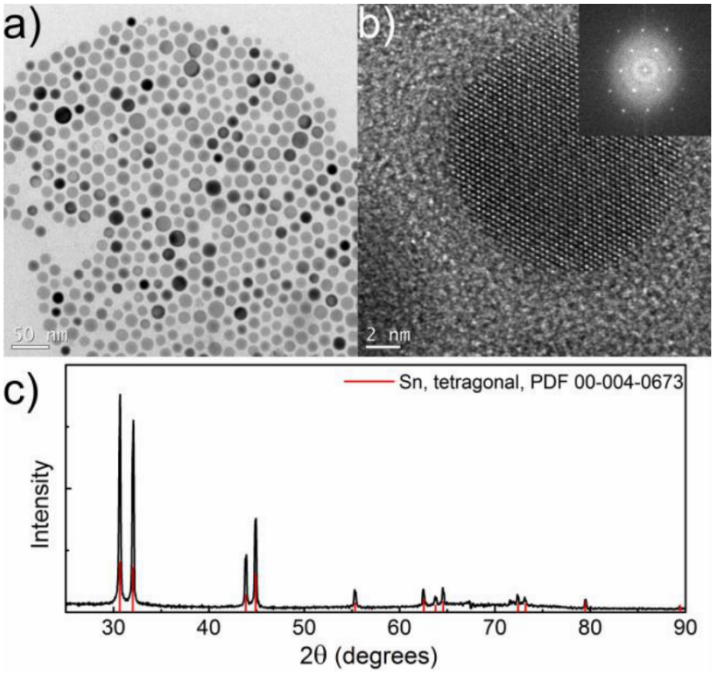

Figure 1.(a) Low-resolution TEM and (b) high-resolution TEM of tin nanocrystals used as seeds for the supercritical fluid-based growth of $Si_{1-x}Ge_x$ nanowires. (c) XRD of tin nanocrystals (Sn PDF: 00-004-0673). (Figure courtesy of Elena Pandres).

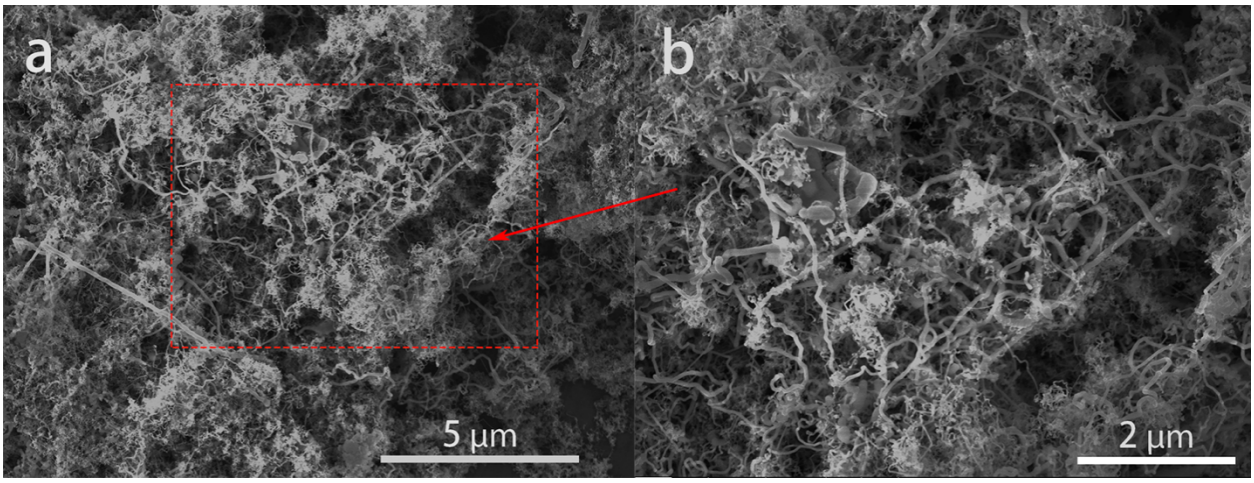

Figure 2. (a) Low magnification SEM of tin-seeded $Si_{1-x}Ge_x$ nanowires. (b) high magnification SEM image of the area outlined in the red dashed box in (a).

Figure 2 shows SEM images of the resulting tin-seeded nanowires. The product of the synthesis contained a few straight nanowires, but the majority of the nanowires were tortuous, which often occurs when precursor kinetics and diffusion do not match the rate of crystallization of the nanowire.[68,69] In addition, large isotropic particles were present in this sample, which likely results from mismatched precursor decomposition kinetics and nanowire growth kinetics. The resulting nanowires are curly with diameters ranging from about 20 to 200 nm. $Si_{1-x}Ge_x$ nanowires lengths can reach well over 10 µm.

3.2 Evidence of $Si_{1-x}Ge_x$ alloying in nanowires

The presence of silicon and germanium alloying, rather than a mixture of pure silicon and pure germanium, was confirmed by both XRD (Figure 3) and Raman Scattering (Figure 4).

Figure 3 shows XRD spectra of $Si_{1-x}Ge_x$ nanowires, highlighting (111) reflection. According to the powder files of Ge and Si, the expected (111) reflection should be located at 27.28° and 28.42°. The peak position was located at 27.8°, corresponding to a d-spacing of 3.2 Å, which is between the one of Si (3.14 Å) and Ge (3.26 Å), indicating successful $Si_{1-x}Ge_x$ alloying.

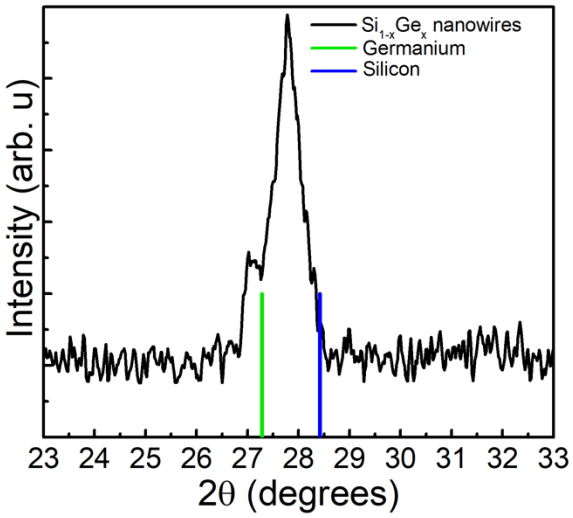

Figure 3. X-ray diffraction of the (111) reflection of $Si_{1-x}Ge_x$ nanowires. The (111) reflection of germanium and silicon from the powder diffraction files are presented as green and blue lines, respectively. Germanium PDF 00-004-0545, silicon PDF 00-005-0565. (Figure courtesy of Elena Pandres)

Three obvious bands are present in both Raman spectra (Figure 4a and Figure 4b). and correspond with the Ge-Ge band, Ge-Si band, and the Si-Si band. For alloyed $Si_{1-x}Ge_x$, a downshift was expected for both Ge-Ge bands and Si-Si bands due to the lattice strain associated with alloying, compared with pure Si (~305 cm^{-1}) and Ge (~520 cm^{-1}). Both theory and experimental data have demonstrated that the Si-Si band is most sensitive to the Ge concentration and downshifts linearly with increasing Ge composition.[70,71] Therefore, the $Si_{1-x}Ge_x$ alloy composition can be calculated from the shift of the Si-Si peak.[71] $Si_{1-x}Ge_x$ alloyed nanowires synthesized from 90 mM monophenylsilane and 5.4 mM triphenylgermane with 0.20 mg/mL tin nanocrystals at 460°C (Figure 4a, Figure 7b) had a Si-Si band position of ~478 cm^{-1}, corresponding with a nanowire composition of $Si_{0.42}Ge_{0.58}$. Raman spectra of another $Si_{1-x}Ge_x$ nanowire synthesis (112 mM monophenylsilane, 6.75 mM triphenylgermane, 0.40 mg/mL Sn nanocrystals, 460°C) had a Si-Si band at 487 cm^{-1} (Figure 4b), corresponding with a nanowire

composition of $Si_{0.55}Ge_{0.45}$. The different Si:Ge ratios of the two nanowire samples demonstrates the potential of further developing a highly tunable $Si_{1-x}Ge_x$ nanowire synthesis through supercritical fluid-based methods by adjusting the reaction conditions.

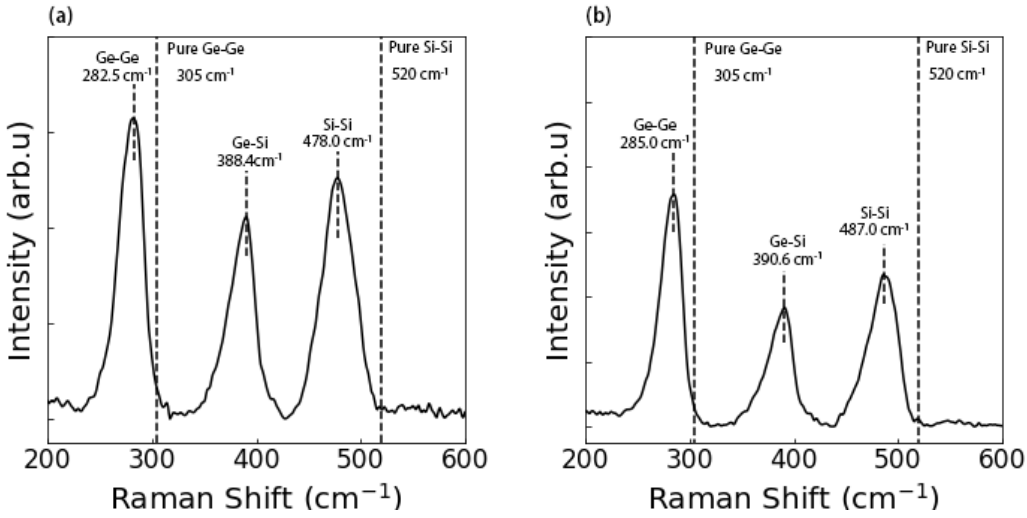

Figure 4. Raman spectra of $Si_{1-x}Ge_x$ nanowire from two different syntheses. (a) $Si_{1-x}Ge_x$ nanowire obtained at 460℃ from [PS: TPG] = 90 mM: 5.4 mM with 0.20 mg/mL tin nanocrystals. (b) $Si_{1-x}Ge_x$ nanowires synthesized at 460℃ from [PS: TPG] = 112 mM: 6.75 mM with 0.40 mg/mL tin nanocrystals. Three prominent peaks were observed, representing the Ge-Ge band (305 cm^{-1}), Ge-Si band (400 cm^{-1}), and Si-Si band (520 cm^{-1}), respectively.

To investigate the elemental distribution throughout the sample, SEM-EDS was performed (Figure 5). The qualitative map of Ge (Figure 5c) and Si (Figure 5d) suggest a uniform $Si_{1-x}Ge_x$ alloy composition throughout the nanowires. According to the spectrum (Figure 5b), the quantitative atomic ratio of Si:Ge would be at 2.5:4.5. To avoid interference from the substrate and accurately measure the silicon atomic ratio, the sample was prepared by dropping dilute nanowires onto aluminum foil, causing the aluminum signal to dominate the spectrum.

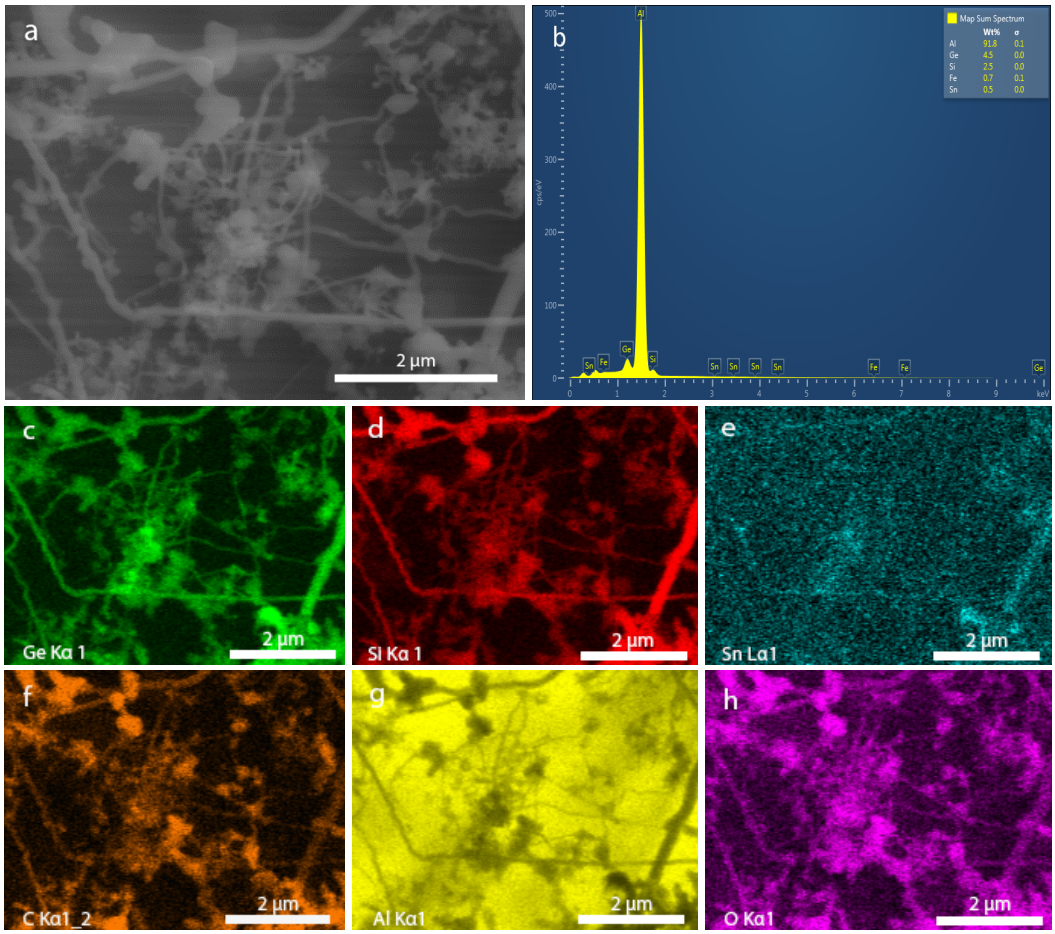

Figure 5.(a) SEM image of Sn-seeded $Si_{1-x}Ge_x$ nanowires obtained from 112 mM monophenylsilane, 6.75 mM triphenylgermane, and 0.52 mg/mL of Sn nanocrystals at 490°C. (b) EDS profile and atomic ratio of elements. (c-h) The corresponding mapping images of each element.

Figure 6 shows SEM-EDS and Raman Scattering of the same $Si_{1-x}Ge_x$ sample (180 mM monophenylsilane, 10.8 mM triphenylgermane, 0.26 mg/mL Sn nanocrystals, 480°C). Based on the Si-Si band peak position at 488 cm^{-1} from Raman Scattering (Figure 6e), the estimated nanowire composition would be at $Si_{0.50}Ge_{0.50}$. Interestingly, the quantitative atomic ratio of Si:Ge (4.6:2.3) from SEM-EDS (Figure 6b) is different than what was calculated from Raman (Figure 6e). In previous work, silicon nanowires resulting from phenylsilane precursor in supercritical fluid-based syntheses were demonstrated to have an amorphous poly(phenylsilane)

coating around the surface. However, since the coated amorphous poly(phenylsilane) would not be incorporated into the crystalline nanowires, it will not contribute to alloying. Therefore, the shift of the peaks in Raman would not be influence by coated shell. While the EDS will only tell you the total ratio of elements present in the sample and the overall spatial distribution, Raman will give you the composition of the elements within the $Si_{1-x}Ge_x$ alloy itself, which could differ substantially from the EDS.

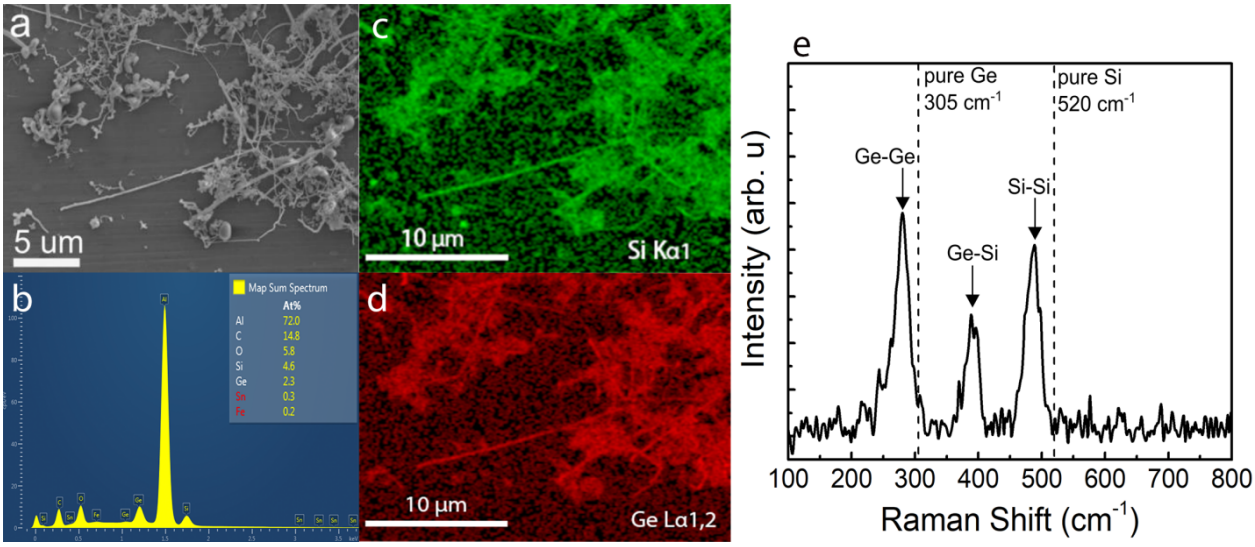

Figure 6.(a) SEM image of Sn-seeded $Si_{1-x}Ge_x$ nanowires obtained from 180 mM monophenylsilane, 10.8 mM triphenylgermane, and 0.26 mg/mL of Sn nanocrystals at 480°C. (b) EDS profile and atomic ratio of elements. (c-d) The corresponding mapping images of silicon and germanium. (e) Raman spectra of the resulting $Si_{1-x}Ge_x$ nanowires. (Figure courtesy of Elena Pandres)

3.3 Effects of Reaction Parameters on $Si_{1-x}Ge_x$ Nanowires

Here, phenylsilane and triphenylgermane were used as the Si and Ge precursors, respectively. The degree of phenyl substitution for each precursor was intentionally chosen due

to the higher reactivity of aryl-germane precursors compared to aryl-silane precursors.[56] By using a greater degree of phenyl substitution on the Ge precursor, the decomposition kinetics of triphenylgermane better match the decomposition kinetics of monophenlysilane, enabling a more balanced disproportionation reaction of the Si and Ge precursors.

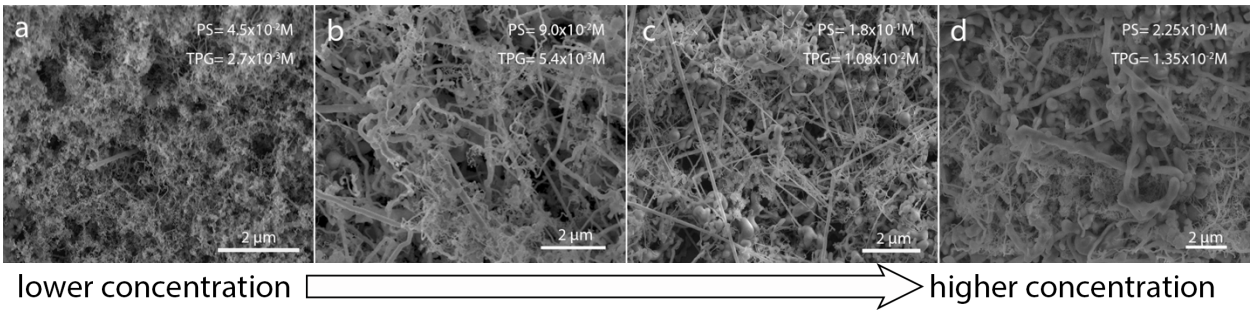

Figure 7.(a-d) SEM images of supercritical-fluid-grown $Si_{1-x}Ge_x$ nanowires grown at 460°C with 0.26 mg/mL tin nanocrystals, with a range of different precursor concentrations. (a) 45 mM monophenylsilane: 2.7 mM triphenylgermane; (b) 90 mM monophenylsilane: 5.4 mM triphenylgermane, (c) 180 mM monophenylsilane: 10.8 mM triphenylgermane, (d) 225 mM monophenylsilane: 13.5 mM triphenylgermane, respectively. A 17:1 ratio of monophenylsilane: triphenylgermane was maintained for all the samples.

Figure 7 shows SEM images of $Si_{1-x}Ge_x$ nanowires synthesized by SFLS-growth at 460°C and with various precursor concentrations. When the synthesis was operated at a higher concentration at [PS: TPG] = 225 mM: 13.5 mM (Figure 7d), straight nanowires with several micrometers in length were surrounded by large isotropic particles. Isotropic particles are a result of homogeneous nucleation, which occurs when the precursor decomposition rate is faster than (1) the rate of semiconductor atoms diffusing to the metal seed to facilitate the anisotropic growth and/or (2) the rate of nanowire crystallization from the seed. In order to balance the kinetics and reduce the isotropic particle formation, we have investigated various reaction parameters, including the overall precursor concentration.

Decreasing the concentration of monophenylsilane and triphenylgermane, while maintaining a consistent ratio of monophenylsilane: triphenylgermane reduces the presence of isotropic particles considerably (Figure 7). However, under the relatively dilute precursor condition (Figure 7a), the resulting nanowires are primarily tortuous and appear to be shorter in length. Although decreasing the precursor concentration may prevent homogenous nucleation and growth of isotropic particles, it may result in nanowires with more defects with a tortuous morphology (Figure 7a). Strategies to minimize the formation of isotropic particles while improving the nanowire morphology could include adjusting the flow rate, the reaction temperature, the ratio of monophenylsilane to triphenylgermane, the ratio of precursors to tin seeds nanocrystals, and the solvent.

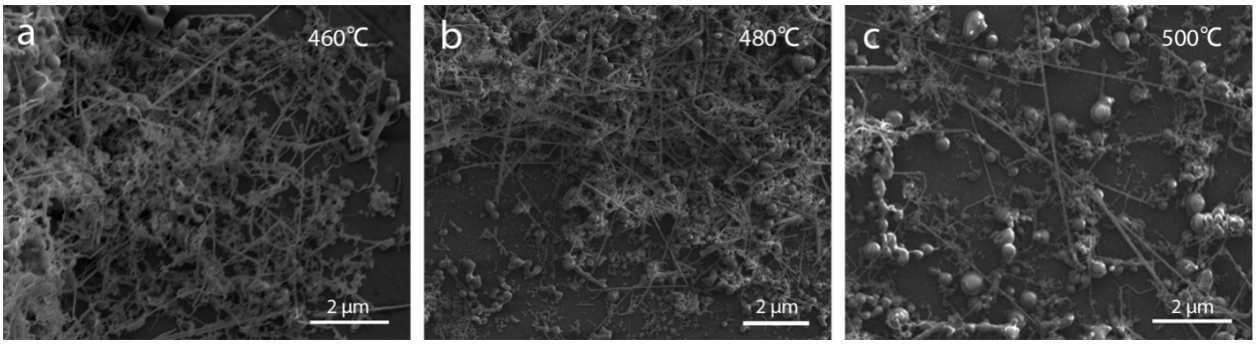

Figure 8. SEM images of $Si_{1-x}Ge_x$ nanowires synthesized with 180 mM phenylsilane and 10.2 mM triphenylgermane at (a) 460℃, (b) 480℃, (c) 500℃.

The reaction temperature plays an important role in supercritical fluid-based nanowire synthesis; it can influence the morphology of nanowires and the formation of byproducts[48,56–58]. Figure 8(a), (b) and (c) show SEM images of the reaction products synthesized from [PS: TPG] = 180 mM: 10.2 mM at different reduction temperatures of 460℃, 480℃ and 500℃ respectively. Figure 8a shows many tortuous nanowires with few isotropic particles. Higher reaction

temperatures produce straighter and longer nanowires at the expense of producing more isotropic particles (Figure 8b). However, at 500°C (Figure 8c), only a small number of nanowires were present, and the majority of the product consisted of isotropic particles—a result of mismatched precursor kinetics and nanowire growth kinetics.

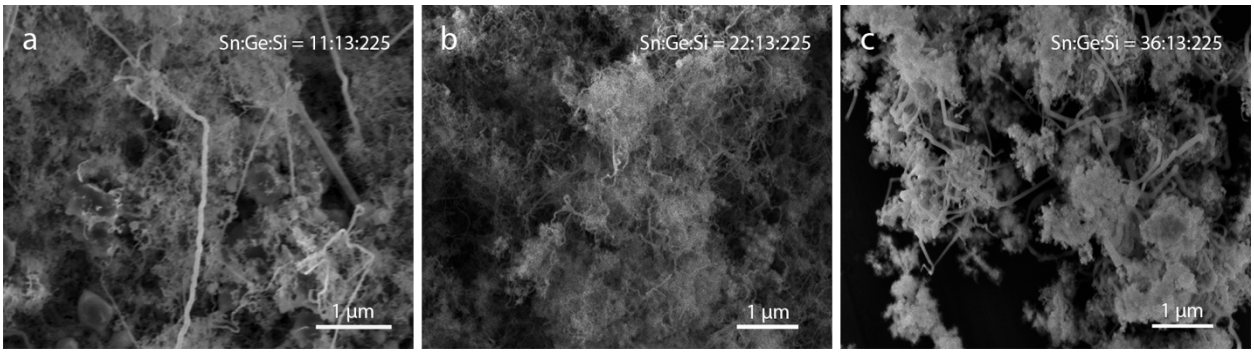

Figure 9. SEM images of $Si_{1-x}Ge_x$ nanowires obtained from [PS: TPG] =112 mM: 6.75 mM in supercritical toluene at 900 psig and 490°C with different molar ratios of Sn:Ge:Si at (a) 11:13:225, (b) 22:13:225, (c) 36:13:225.

The metal seed to precursor ratio is another important reaction parameter that influences the quality of nanowires in supercritical fluid-based syntheses[55,59]. Figure 9 shows images of $Si_{1-x}Ge_x$ nanowires synthesized with different Sn:Ge:Si ratios. A relatively low Sn:Ge:Si ratio (11:13:225) resulted in a combination of tortuous and straight nanowires as well as isotropic particles (Figure 9a). Increasing the Sn:Ge:Si ratio (22:13:225) decreased the number of isotropic particles and produced more tortuous nanowires (Figure 9b). However, relatively high Sn:Ge:Si ratios (36:13:225) resulted in few tortuous nanowires and with many smaller isotropic particles showing. The size of the isotropic particles in Figure 9c are much smaller and aggregated, compared to the large isotropic particles in Figure 9a.

Chapter 4. CONCLUSIONS

To our knowledge, this is the first successful synthesis of alloyed $Si_{1-x}Ge_x$ nanowires via a supercritical fluid-based process. XRD and Raman spectroscopy confirmed alloying throughout $Si_{1-x}Ge_x$ nanowires. A uniform distribution of silicon and germanium throughout the nanowires was observed through SEM-EDS mapping. Moreover, shifts in the Raman bands enabled estimation of the nanowire composition for two different samples ($Si_{0.42}Ge_{0.58}$ and $Si_{0.55}Ge_{0.45}$). The different nanowire compositions suggest that the supercritical fluid-based synthesis can be developed further to tune the ratio of silicon to germanium in $Si_{1-x}Ge_x$ alloyed nanowires. In addition, the discrepancy of estimated $Si_{1-x}Ge_x$ composition from Raman with the SEM-EDS suggesting a coating shell (poly(phenylsilane)) existing around the nanowire.

Reaction conditions such as temperature, precursor concentration and metal seed to precursor ratio play key roles in the resulting product morphology. Both high precursor concentration and high reaction temperature result in a combination of isotropic particles as well as straight and long nanowires due to mismatched kinetics. Decreasing the overall precursor concentration and temperature minimizes homogeneous nucleation of isotropic particles but results in a tortuous nanowire morphology. For applications in which the nanowire morphology is especially important, the balance between the reaction conditions will require further investigations in order to produce $Si_{1-x}Ge_x$ nanowires without byproducts such as isotropic particles.

Chapter 5. FUTURE DIRECTIONS

Although this work improves upon the compositional control of supercritical fluid-grown semiconductor nanowires, further work is still necessary in order to minimize homogeneous nucleation of isotropic particles and to produce primarily alloyed $Si_{1-x}Ge_x$ nanowires. Future work should be focused on identifying the balance among the parameters researched here—reaction temperature, overall precursor concentration, and metal seed to precursor ratio—to reduce the presence of isotropic particles. In addition, reaction parameters such as flow rate, solvent choice, and degree of phenyl substitution of aryl precursors should be investigated to improve the production of alloyed nanowires and minimize formation of isotropic particles. Furthermore, this supercritical fluid-based synthesis should be developed to tune the Si:Ge ratio of the nanowires. In order to adjust the Si:Ge ratio, the silicon to germanium precursor ratio as well as the degree of phenyl substitution should be explored. Eventually, with the ability to tune the Si:Ge ratio of $Si_{1-x}Ge_x$ nanowires through a scalable process, we plan to integrate these nanomaterials into electrodes and test capacity, rate capability, and lithium diffusion as a function of $Si_{1-x}Ge_x$ composition.

BIBLIOGRAPHY

1. Su, X. et al. Silicon-Based Nanomaterials for Lithium-Ion Batteries: A Review. Adv. Energy Mater. 4, 1300882 (2014).
2. Zhang, W.-J. A review of the electrochemical performance of alloy anodes for lithium-ion batteries. J. Power Sources 196, 13–24 (2011).
3. Wu, H. & Cui, Y. Designing nanostructured Si anodes for high energy lithium ion batteries. Nano Today 7, 414–429 (2012).
4. Bates, J. B., Dudney, N. J., Neudecker, B., Ueda, A. & Evans, C. D. Thin-film lithium and lithium-ion batteries. Solid State Ion. 135, 33–45 (2000).
5. Li, H., Wang, Z., Chen, L. & Huang, X. Research on Advanced Materials for Li-ion Batteries. Adv. Mater. 21, 4593–4607 (2009).
6. Wu, H. et al. Stable cycling of double-walled silicon nanotube battery anodes through solid–electrolyte interphase control. Nat. Nanotechnol. 7, 310–315 (2012).
7. Raić, M. et al. Nanostructured Silicon as Potential Anode Material for Li-Ion Batteries. Molecules 25, 891 (2020).
8. Wu, H. et al. Stable Li-ion battery anodes by in-situ polymerization of conducting hydrogel to conformally coat silicon nanoparticles. Nat. Commun. 4, 1943 (2013).
9. Silicon Nanotube Battery Anodes | Nano Letters.
10. Abel, P. R. et al. Nanostructured Si(1-x)Gex for Tunable Thin Film Lithium-Ion Battery Anodes. ACS Nano 7, 2249–2257 (2013).
11. Chan, C. K. et al. High-performance lithium battery anodes using silicon nanowires. Nat. Nanotechnol. 3, 31–35 (2008).
12. Choi, N.-S., Yao, Y., Cui, Y. & Cho, J. One dimensional Si/Sn - based nanowires and

nanotubes for lithium-ion energy storage materials. J. Mater. Chem. 21, 9825–9840 (2011).

13. Graetz, J., Ahn, C. C., Yazami, R. & Fultz, B. Highly Reversible Lithium Storage in Nanostructured Silicon. Electrochem. Solid State Lett. 6, A194 (2003).

14. Gao, B., Sinha, S., Fleming, L. & Zhou, O. Alloy Formation in Nanostructured Silicon. Adv. Mater. 13, 816–819 (2001).

15. Kasavajjula, U., Wang, C. & Appleby, A. J. Nano- and bulk-silicon-based insertion anodes for lithium-ion secondary cells. J. Power Sources 163, 1003–1039 (2007).

16. Chockla, A. M. et al. Electrochemical Lithiation of Graphene-Supported Silicon and Germanium for Rechargeable Batteries. J. Phys. Chem. C 116, 11917–11923 (2012).

17. Xue, D.-J. et al. Improving the Electrode Performance of Ge through Ge@C Core–Shell Nanoparticles and Graphene Networks. J. Am. Chem. Soc. 134, 2512–2515 (2012).

18. Yang, L. C., Gao, Q. S., Li, L., Tang, Y. & Wu, Y. P. Mesoporous germanium as anode material of high capacity and good cycling prepared by a mechanochemical reaction. Electrochem. Commun. 12, 418–421 (2010).

19. Park, M.-H., Kim, K., Kim, J. & Cho, J. Flexible Dimensional Control of High-Capacity Li-Ion-Battery Anodes: From 0D Hollow to 3D Porous Germanium Nanoparticle Assemblies. Adv. Mater. 22, 415–418 (2010).

20. Wang, D. et al. Surface Chemistry and Electrical Properties of Germanium Nanowires. J. Am. Chem. Soc. 126, 11602–11611 (2004).

21. Kennedy, T. et al. High-Performance Germanium Nanowire-Based Lithium-Ion Battery Anodes Extending over 1000 Cycles Through in Situ Formation of a Continuous Porous Network. Nano Lett. 14, 716–723 (2014).

22. Hannon, J. B., Kodambaka, S., Ross, F. M. & Tromp, R. M. The influence of the surface migration of gold on the growth of silicon nanowires. Nature 440, 69–71 (2006).

23. Kodambaka, S., Hannon, J. B., Tromp, R. M. & Ross, F. M. Control of Si Nanowire Growth by Oxygen. Nano Lett. 6, 1292–1296 (2006).

24. Allen, J. E. et al. High-resolution detection of Au catalyst atoms in Si nanowires. Nat. Nanotechnol. 3, 168–173 (2008).

25. Moutanabbir, O. et al. Colossal injection of catalyst atoms into silicon nanowires. Nature 496, 78–82 (2013).

26. Shin, N. & Filler, M. A. Controlling Silicon Nanowire Growth Direction via Surface Chemistry. Nano Lett. 12, 2865–2870 (2012).

27. Wagner, R. S. & Ellis, W. C. Vapor-liquid-solid mechanism of single crystal growth. Appl. Phys. Lett. 4, 89–90 (1964).

28. Cui, Y., Lauhon, L. J., Gudiksen, M. S., Wang, J. & Lieber, C. M. Diameter-controlled synthesis of single-crystal silicon nanowires. Appl. Phys. Lett. 78, 2214–2216 (2001).

29. Nebol'sin, V. A., Shchetinin, A. A., Dolgachev, A. A. & Korneeva, V. V. Effect of the Nature of the Metal Solvent on the Vapor-Liquid-Solid Growth Rate of Silicon Whiskers. Inorg. Mater. 41, 1256–1259 (2005).

30. Park, W. I., Zheng, G., Jiang, X., Tian, B. & Lieber, C. M. Controlled Synthesis of Millimeter-Long Silicon Nanowires with Uniform Electronic Properties. Nano Lett. 8, 3004–3009 (2008).

31. Schubert, L. et al. Silicon nanowhiskers grown on 〈111〉 Si substrates by molecular-beam epitaxy. Appl. Phys. Lett. 84, 4968–4970 (2004).

32. Das Kanungo, P. et al. Controlled in situ boron doping of short silicon nanowires grown

by molecular beam epitaxy. Appl. Phys. Lett. 92, 263107 (2008).

33. Zakharov, N. D. et al. Growth phenomena of Si and Si/Ge nanowires on Si (111) by molecular beam epitaxy. J. Cryst. Growth 290, 6–10 (2006).

34. Zhang, Y. F. et al. Silicon nanowires prepared by laser ablation at high temperature. Appl. Phys. Lett. 72, 1835–1837 (1998).

35. Zhou, G. W., Zhang, Z., Bai, Z. G., Feng, S. Q. & Yu, D. P. Transmission electron microscopy study of Si nanowires. Appl. Phys. Lett. 73, 677–679 (1998).

36. Zhang, Y. F. et al. Diameter modification of silicon nanowires by ambient gas. Appl. Phys. Lett. 75, 1842–1844 (1999).

37. Yang, Y.-H., Wu, S.-J., Chiu, H.-S., Lin, P.-I. & Chen, Y.-T. Catalytic Growth of Silicon Nanowires Assisted by Laser Ablation. J. Phys. Chem. B 108, 846–852 (2004).

38. Schmidt, V., Wittemann, J. V., Senz, S. & Gösele, U. Silicon Nanowires: A Review on Aspects of their Growth and their Electrical Properties. Adv. Mater. 21, 2681–2702 (2009).

39. Trentler, T. J. et al. Solution-Liquid-Solid Growth of Crystalline III-V Semiconductors: An Analogy to Vapor-Liquid-Solid Growth. Science 270, 1791–1794 (1995).

40. Wang, F. et al. Solution−Liquid−Solid Growth of Semiconductor Nanowires. Inorg. Chem. 45, 7511–7521 (2006).

41. Dong, A., Yu, H., Wang, F. & Buhro, W. E. Colloidal GaAs Quantum Wires: Solution−Liquid−Solid Synthesis and Quantum-Confinement Studies. J. Am. Chem. Soc. 130, 5954–5961 (2008).

42. Sun, J., Liu, C. & Yang, P. Surfactant-Free, Large-Scale, Solution–Liquid–Solid Growth of Gallium Phosphide Nanowires and Their Use for Visible-Light-Driven Hydrogen

Production from Water Reduction. J. Am. Chem. Soc. 133, 19306–19309 (2011).

43. Laocharoensuk, R. et al. Flow-based solution–liquid–solid nanowire synthesis. Nat. Nanotechnol. 8, 660–666 (2013).

44. Lu, X., Hessel, C. M., Yu, Y., Bogart, T. D. & Korgel, B. A. Colloidal Luminescent Silicon Nanorods. Nano Lett. 13, 3101–3105 (2013).

45. Yu, H. et al. Cadmium Selenide Quantum Wires and the Transition from 3D to 2D Confinement. J. Am. Chem. Soc. 125, 16168–16169 (2003).

46. Grebinski, J. W., Hull, K. L., Zhang, J., Kosel, T. H. & Kuno, M. Solution-Based Straight and Branched CdSe Nanowires. Chem. Mater. 16, 5260–5272 (2004).

47. Fanfair, D. D. & Korgel, B. A. Bismuth Nanocrystal-Seeded III-V Semiconductor Nanowire Synthesis. Cryst. Growth Des. 5, 1971–1976 (2005).

48. Holmes, J. D., Johnston, K. P., Doty, R. C. & Korgel, B. A. Control of Thickness and Orientation of Solution-Grown Silicon Nanowires. Science 287, 1471–1473 (2000).

49. Lu, X., Harris, J. T., Villarreal, J. E., Chockla, A. M. & Korgel, B. A. Enhanced Nickel-Seeded Synthesis of Germanium Nanowires. Chem. Mater. 25, 2172–2177 (2013).

50. Hanrath, T. & Korgel, B. A. Nucleation and Growth of Germanium Nanowires Seeded by Organic Monolayer-Coated Gold Nanocrystals. J. Am. Chem. Soc. 124, 1424–1429 (2002).

51. Chockla, A. M. et al. Influences of Gold, Binder and Electrolyte on Silicon Nanowire Performance in Li-Ion Batteries. J. Phys. Chem. C 116, 18079–18086 (2012).

52. Davidson, F. M., Schricker, A. D., Wiacek, R. J. & Korgel, B. A. Supercritical Fluid–Liquid–Solid Synthesis of Gallium Arsenide Nanowires Seeded by Alkanethiol-Stabilized Gold Nanocrystals. Adv. Mater. 16, 646–649 (2004).

53. Supercritical Fluid–Liquid–Solid (SFLS) Synthesis of Si and Ge Nanowires Seeded by Colloidal Metal Nanocrystals - Hanrath - 2003 - Advanced Materials - Wiley Online Library.

54. Supercritical Fluid−Liquid−Solid Synthesis of Gallium Phosphide Nanowires | Chemistry of Materials.

55. Yuan, F.-W., Yang, H.-J. & Tuan, H.-Y. Alkanethiol-Passivated Ge Nanowires as High-Performance Anode Materials for Lithium-Ion Batteries: The Role of Chemical Surface Functionalization. ACS Nano 6, 9932–9942 (2012).

56. Chockla, A. M., Klavetter, K. C., Mullins, C. B. & Korgel, B. A. Tin-Seeded Silicon Nanowires for High Capacity Li-Ion Batteries. Chem. Mater. 24, 3738–3745 (2012).

57. Chan, C. K., Patel, R. N., O'Connell, M. J., Korgel, B. A. & Cui, Y. Solution-Grown Silicon Nanowires for Lithium-Ion Battery Anodes. ACS Nano 4, 1443–1450 (2010).

58. Chockla, A. M. et al. Silicon Nanowire Fabric as a Lithium Ion Battery Electrode Material. J. Am. Chem. Soc. 133, 20914–20921 (2011).

59. Xiao, W., Zhou, J., Yu, L., Wang, D. & Lou, X. W. (David). Electrolytic Formation of Crystalline Silicon/Germanium Alloy Nanotubes and Hollow Particles with Enhanced Lithium-Storage Properties. Angew. Chem. 128, 7553–7557 (2016).

60. Kim, H. et al. Germanium Silicon Alloy Anode Material Capable of Tunable Overpotential by Nanoscale Si Segregation. Nano Lett. 15, 4135–4142 (2015).

61. Yang, Y. et al. Morphology- and Porosity-Tunable Synthesis of 3D Nanoporous SiGe Alloy as a High-Performance Lithium-Ion Battery Anode. ACS Nano 12, 2900–2908 (2018).

62. Mullane, E., Geaney, H. & M. Ryan, K. Synthesis of silicon–germanium axial nanowire

heterostructures in a solvent vapor growth system using indium and tin catalysts. Phys. Chem. Chem. Phys. 17, 6919–6924 (2015).

63. Stokes, K. et al. Direct Synthesis of Alloyed Si1–xGex Nanowires for Performance-Tunable Lithium Ion Battery Anodes. ACS Nano 11, 10088–10096 (2017).

64. Kennedy, T. et al. Nanowire Heterostructures Comprising Germanium Stems and Silicon Branches as High-Capacity Li-Ion Anodes with Tunable Rate Capability. ACS Nano 9, 7456–7465 (2015).

65. Tuan, H.-Y., Lee, D. C. & Korgel, B. A. Nanocrystal-Mediated Crystallization of Silicon and Germanium Nanowires in Organic Solvents: The Role of Catalysis and Solid-Phase Seeding. Angew. Chem. Int. Ed. 45, 5184–5187 (2006).

66. Tuan, H.-Y., Lee, D. C., Hanrath, T. & Korgel, B. A. Germanium Nanowire Synthesis: An Example of Solid-Phase Seeded Growth with Nickel Nanocrystals. Chem. Mater. 17, 5705–5711 (2005).

67. Kravchyk, K. et al. Monodisperse and Inorganically Capped Sn and Sn/SnO2 Nanocrystals for High-Performance Li-Ion Battery Anodes. J. Am. Chem. Soc. 135, 4199–4202 (2013).

68. Lee, D. C., Hanrath, T. & Korgel, B. A. The Role of Precursor-Decomposition Kinetics in Silicon-Nanowire Synthesis in Organic Solvents. Angew. Chem. Int. Ed. 44, 3573–3577 (2005).

69. Lu, X., Hanrath, T., Johnston, K. P. & Korgel, B. A. Growth of Single Crystal Silicon Nanowires in Supercritical Solution from Tethered Gold Particles on a Silicon Substrate. Nano Lett. 3, 93–99 (2003).

70. Ren, S.-F., Cheng, W. & Yu, P. Y. Microscopic investigation of phonon modes in SiGe

alloy nanocrystals. Phys. Rev. B 69, 235327 (2004).

71. Lu, Q. et al. Raman Scattering from Si1-xGex Alloy Nanowires. J. Phys. Chem. C 112, 3209–3215 (2008).